Proteasome Inhibition Enhances Lysosome-mediated Targeted Protein Degradation

Ahmed M. Elshazly[1,2,3], Nayyerehalsadat Hosseini[1], Shanwei Shen[1], Victoria Neely[4], Hisashi Harada[4,6], Steven Grant[5,6], Senthil K. Radhakrishnan[1,6*]

[1]Department of Pathology,
Virginia Commonwealth University, Richmond, Virginia, USA

[2]Department of Pharmacology and Toxicology,
Virginia Commonwealth University, Richmond, Virginia, USA

[3]Department of Pharmacology and Toxicology,
Faculty of Pharmacy, Kafrelsheikh University, Kafrelsheikh, Egypt

[4]Philips Institute for Oral Health Research, School of Dentistry,
Virginia Commonwealth University, Richmond, Virginia, USA

[5]Division of Hematology and Oncology, Department of Internal Medicine,
Virginia Commonwealth University, Richmond, Virginia, USA

[6]Massey Comprehensive Cancer Center,
Virginia Commonwealth University, Richmond, Virginia, USA

Running Title: Lysosome-mediated Targeted Protein Degradation (TPD)

Keywords: AUTAC, TPD, proteasome inhibitor, NRF1, NFE2L1, Mcl1, cancer

*Correspondence:
Senthil K. Radhakrishnan
Senthil.Radhakrishnan@vcuhealth.org

ABSTRACT

Proteasome inhibitor drugs are currently used in the clinic to treat multiple myeloma and mantle cell lymphoma. These inhibitors cause accumulation of undegraded proteins, thus inducing proteotoxic stress and consequent cell death. However, cancer cells counteract this effect by activating an adaptive response through the transcription factor Nuclear factor erythroid 2-related factor 1 (NRF1, also known as NFE2L1). NRF1 induces transcriptional upregulation of proteasome and autophagy/lysosomal genes, thereby reducing proteotoxic stress and diminishing the effectiveness of proteasome inhibition. While suppressing this protective autophagy response is one potential strategy, here we investigated whether this heightened autophagy could instead be leveraged therapeutically. To this end, we designed an autophagy-targeting chimera (AUTAC) compound to selectively degrade the anti-apoptotic protein Mcl1 via the lysosome. Our results show that this lysosome-mediated targeted degradation is significantly amplified in the presence of proteasome inhibition, in a NRF1-dependent manner. The combination of the proteasome inhibitor carfilzomib and Mcl1 AUTAC synergistically promoted cell death in both wild-type and proteasome inhibitor-resistant multiple myeloma and lung cancer cells. Thus, our work offers a novel strategy for enhancing proteasome inhibitor efficacy by exploiting the adaptive autophagy response. More broadly, our study establishes a framework for amplifying lysosome-mediated targeted protein degradation, with potential applications in cancer therapeutics and beyond.

INTRODUCTION

Proteasome inhibitors (PIs) are a cornerstone in the treatment of multiple myeloma and are also part of mantle cell lymphoma therapeutic protocols [1,2]. FDA-approved PIs—bortezomib, carfilzomib, and ixazomib—are small-molecule inhibitors designed to target the proteasome. Bortezomib and ixazomib are peptide boronate inhibitors, mimicking proteasome substrates through dipeptide-like structures, while carfilzomib is an epoxyketone-based inhibitor that binds irreversibly to the β5 subunit [3]. By blocking proteasomal activity, these drugs induce endoplasmic reticulum (ER) stress due to the accumulation of unfolded proteins and insoluble aggregates, which ultimately leads to cell cycle arrest, activation of antiproliferative signals, and apoptosis [1,4,5]. While PIs have demonstrated clinical success in blood malignancies, they have shown limited efficacy against solid tumors [6-11]. Additionally, their long-term utility is often hindered by the development of resistance, leading to relapse and poor prognosis [12].

Tumor cells activate a range of adaptive mechanisms to counteract the cytotoxic effects of PIs, including the activation of nuclear factor erythroid 2-related factor 1 (NRF1, also known as NFE2L1). NRF1 resides in the ER membrane as an inactive p120 precursor and is cleaved by the protease DDI2 to its active p110 form upon proteasome inhibition. The active NRF1 translocates to the nucleus, where it upregulates the expression of proteasome and autophagy/lysosomal genes, thereby mitigating proteotoxic stress and reducing PI efficacy [13-15]. Although directly targeting NRF1 remains challenging due to the complexity of its pathway, adaptive responses such as NRF1-mediated autophagy induction could represent potential therapeutic vulnerabilities. Autophagy, a cytoplasmic recycling process critical for maintaining cellular homeostasis, enables tumor cells to survive under chemotherapeutic stress – a phenomenon referred to as cytoprotective autophagy [16,17]. Multiple studies have linked autophagy activation to PI resistance development [18-21]. Instead of inhibiting autophagy, here we sought to exploit this cytoprotective mechanism for therapeutic benefit using autophagy-targeting chimera (AUTAC) technology. AUTACs rely on cGMP-mediated S-guanylation, which has been implicated in the selective autophagic degradation of Group A Streptococcus (GAS) [22]. These compounds consist of an autophagy degradation tag, typically fluorobenzyl guanine (FBnG) derivatives, linked to a ligand that targets a specific protein of interest [23].

The anti-apoptotic protein Mcl1, a key regulator of mitochondrial integrity, binds and sequesters pro-apoptotic proteins such as Bax, Bak, and Bok, thereby preventing cytochrome C release and apoptosis [24,25]. Elevated Mcl1 levels following proteasome inhibition contribute to PI resistance in multiple myeloma [26-28]. Preclinical studies have shown that suppressing Mcl1 restores PI sensitivity [27,29-32], and several clinical trials are underway to evaluate Mcl1 inhibitors in multiple myeloma (NCT04178902, NCT03465540, NCT04543305, NCT02675452, NCT02992483). However, these efforts are constrained by concerns over potential cardiac toxicity [33].

In this study, we developed an AUTAC compound to selectively degrade Mcl1 via the lysosomal pathway. Our results demonstrate that this lysosome-mediated targeted degradation is significantly enhanced by proteasome inhibition in an NRF1-dependent manner. The combination of carfilzomib and Mcl1 AUTAC synergistically induced cell death in both wild-

type and PI-resistant multiple myeloma and non-small cell lung cancer cells. Overall, our findings provide a novel strategy to enhance PI efficacy by leveraging the adaptive autophagy response.

RESULTS

AUTAC-Mediated Degradation of Mcl1 via Autophagic Machinery

Building on the efforts of Arimoto's group [22,23,34] and recognizing the importance of targeting Mcl1, we developed an Mcl1-targeting AUTAC utilizing a second-generation pyrazole-linked FBnG tag. This tag was conjugated via a pyrazole linker to the S1-6 derivative, a well-characterized Mcl1 inhibitor [35] (Fig. 1A). To verify the selectivity of AUTAC, we evaluated its effect on Bcl2 family proteins in the U266B1 cell line across various concentrations (Fig. 1B). AUTAC reduced Mcl1 protein levels in a dose- and time-dependent manner while exerting minimal effects on Bclxl and no observable impact on Bcl2 levels. Additionally, AUTAC increased LC3 I/II levels, indicating activation of the autophagic machinery (Fig. 1B). These results were further confirmed by immunofluorescence staining of U266B1 cells treated with AUTAC for 24 and 48 hours, which revealed a time-dependent reduction in Mcl1 levels, accompanied by LC3B accumulation. Notably, colocalization of Mcl1 and LC3B was observed at 24 hours (Fig. 1C).

To confirm the autophagy-dependent mechanism of AUTAC, we pharmacologically inhibited the autophagic machinery using chloroquine (CQ) [36] and 3-Methyladenine (3-MA) [37]. This inhibition rescued AUTAC-mediated degradation of Mcl1 in U266B1 cells (Fig. 1D). Moreover, combining AUTAC with CQ led to greater LC3 II accumulation compared to CQ alone, consistent with enhanced autophagic flux (Fig. 1D). Genetic knockdown of ATG5 similarly alleviated AUTAC-mediated Mcl1 degradation (Fig. 1E). These findings establish that AUTAC selectively targets Mcl1 for degradation through autophagy.

Next, we assessed the impact of AUTAC-mediated Mcl1 degradation on cell viability. We observed that AUTAC reduced U266B1 cell viability in a time-dependent manner at 5 μM (Fig. 1F). Given the cardiotoxicity associated with Mcl1 inhibitors in clinical trials, we evaluated AUTAC's effect on AC16 cardiomyocytes. AUTAC minimally affected AC16 viability (Fig. 1G), confirming its selective action against tumor cells.

Autophagy Induction Augments the AUTAC-Mediated Degradation of Mcl1

We hypothesized that combining an autophagy inducer with AUTAC could enhance its ability to degrade Mcl1. To test this notion, we induced autophagy in U266B1 cells via starvation [38], which was confirmed by lysotracker staining and the degradation of p62 (Supplementary Fig. 1A and B). Treatment of U266B1 cells with 5 μM AUTAC for 24 hours in conjunction with starvation resulted in more pronounced Mcl1 degradation compared to AUTAC alone (Supplementary Fig. 1B).

Carfilzomib (CFZ), a first-line proteasome inhibitor for relapsed and refractory multiple myeloma [39], has been shown by our group and others to induce autophagy [13,18,19,40]. Consistent with these reports, CFZ treatment induced autophagy in U266B1 cells, as evidenced by lysotracker staining and LC3I/II accumulation (Supplementary Fig. 2A and B). This induction of autophagic flux was also observed in the proteasome inhibitor-resistant U266B1R cells (Supplementary Fig. 2B). We next evaluated the combined effect of CFZ and AUTAC on Mcl1 levels. CFZ enhanced AUTAC-mediated Mcl1 degradation across multiple myeloma cell lines, including U266B1, MM.1S, RPMI-8226, and AMO-1, with a concurrent increase in autophagic flux, as shown by LC3I/II levels (Fig. 2A). Notably, this effect was recapitulated in proteasome inhibitor-resistant multiple myeloma cell lines, such as U266B1^{R} and AMO-1^{R} (Fig. 2B).

We then extended this approach to solid tumor non-small cell lung cancer (NSCLC) cell lines NCI-H1975 and proteasome inhibitor-resistant NCI-H1975^{R}. AUTAC alone demonstrated significant efficacy in degrading Mcl1, accompanied by autophagy induction, as indicated by increased LC3I/II levels (Fig. 2C). The combination of CFZ (2.5 or 10 nM) with AUTAC further enhanced Mcl1 degradation and autophagic responses compared to AUTAC alone in both cell lines (Fig. 2C).

To explore whether CFZ could amplify the Mcl1 degradation achieved with lower doses of AUTAC, we treated U266B1 cells with CFZ (10 nM) in combination with varying AUTAC doses (500 nM, 1 μM, and 5 μM). This combination resulted in greater Mcl1 degradation compared to each dose of AUTAC alone, along with increased autophagic flux confirmed by LC3I/II accumulation (Fig. 2D).

Finally, we validated CFZ's ability to enhance Mcl1 degradation by AUTAC using immunofluorescence staining in U266B1 cells treated with AUTAC and/or CFZ for 16 hours. While AUTAC alone reduced Mcl1 levels, the combination with CFZ led to a more pronounced reduction (Fig. 2 E and F). Both AUTAC and CFZ alone increased LC3B and the lysosomal marker LAMP1 levels, indicative of active autophagic flux; however, the combination treatment resulted in significant accumulation of these markers. Co-localization of Mcl1 with LC3B was observed in U266B1 cells treated with AUTAC alone or in combination with CFZ (Fig. 2E). Taken together, our findings establish that autophagy inducers, particularly CFZ, enhance the ability of AUTACs to degrade Mcl1 via amplifying autophagic flux.

CFZ-mediated Enhancement of AUTAC Activity is Dependent on NRF1 and Functional Autophagy.

We have previously demonstrated that NRF1 is a key regulator of cellular responses to proteotoxic stress induced by proteasome inhibition [41-44]. NRF1 facilitates the upregulation of proteasome genes to restore proteasome activity and promotes autophagy, providing cells with alternative pathways to degrade ubiquitylated protein aggregates. These mechanisms enable cells to mitigate proteotoxic stress. Notably, our group has shown that NRF1 knockout abolishes carfilzomib-induced autophagy, resulting in the accumulation of autophagosome vacuoles in NRF1-deficient cells [13]. To expand on these findings, we assessed the impact of NRF1 knockout on Mcl1 degradation mediated by the combination of AUTAC and CFZ in U266B1 cells. NRF1 knockout reduced CFZ-induced autophagy, as indicated by a decrease in LC3I/II levels (Fig.

3A). Importantly, NRF1 knockout rescued Mcl1 levels, preventing the reduction achieved by the combination of AUTAC and CFZ in wild-type cells. This effect was accompanied by diminished autophagic flux, as evidenced by decreased LC3I/II levels in NRF1-deficient cells compared to wild-type controls (Fig. 3A). To further validate the role of autophagy in this context, we employed an orthogonal approach. Knockdown of ATG5, an essential autophagy gene, significantly attenuated the Mcl1 degradation observed with the CFZ and AUTAC combination in U266B1 cells (Fig. 3B). Together, these findings underscore the pivotal role of NRF1 in CFZ-induced autophagy and highlight the necessity of functional autophagy for the synergistic activity of CFZ and AUTAC in degrading Mcl1.

AUTAC Potentiates CFZ Toxicity in Wild-Type and Proteasome Inhibitor-Resistant Cancer Cells

Chemotherapeutic agents modulate autophagy in distinct ways, including cytotoxic, cytostatic, non-protective, and cytoprotective forms [45-47]. CFZ has been shown to induce cytoprotective autophagy [18-20,40], which we confirmed in our study using autophagy inhibitors like chloroquine (CQ) and bafilomycin (BAF), which enhanced CFZ toxicity in both U266B1 cells and proteasome inhibitor-resistant U266B1^{R} cells (Supplementary Fig. 2B-D).

Given AUTAC's ability to degrade Mcl1 in an autophagy-dependent manner, we hypothesized that combining AUTAC with CFZ could enhance its cytotoxic effects. Indeed, this combination reduced the viability of multiple myeloma cell lines, including U266B1, AMO-1, MM.1S, and RPMI-8226, while also sensitizing resistant lines (U266B1^{R} and AMO-1^{R}) to CFZ (Fig. 4A). Western blot analysis revealed increased cleaved caspase-3 levels, indicating apoptosis induction in both wild-type and resistant cells (Fig. 4B). These findings highlight AUTAC's ability to redirect cytoprotective autophagy toward Mcl1 degradation, ultimately enhancing cell death.

In solid tumors, including non-small cell lung cancer (NSCLC), proteasome inhibitors (PIs) have shown limited efficacy [6-8]. To improve PI efficacy in this context, we evaluated the combination of AUTAC and CFZ in wild-type (NCI-H1975) and bortezomib-resistant (NCI-H1975^{R}) NSCLC cells. The combination significantly reduced cell viability compared to either treatment alone (Fig. 5A) and increased cleaved caspase-3 accumulation, confirming apoptosis (Fig. 5B). Colony formation assays demonstrated that while AUTAC or CFZ alone moderately reduced the colony-forming ability of NCI-H1975 cells, their combination had a significantly stronger effect. In NCI-H1975^{R} cells, which showed minimal response to CFZ alone, the combination markedly inhibited colony formation (Fig. 5C). These findings highlight the potential of AUTAC to enhance PI efficacy by disrupting cytoprotective autophagy and promoting apoptotic cell death in both hematologic and solid tumors.

DISCUSSION

Proteasome inhibitors (PIs) have transformed the treatment landscape for multiple myeloma, eliciting robust initial responses and significantly improving patient outcomes and survival rates. However, disease relapse and acquired resistance remain major clinical challenges

[48]. Several adaptive mechanisms could underlie resistance to PIs, including NRF1-driven autophagy and the antiapoptotic role of Mcl1 [13-15,26-28]. In this study, we demonstrated that leveraging Mcl1-targeting AUTAC enhances the efficacy of CFZ in both hematologic malignancies and solid tumors, including proteasome inhibitor-resistant models.

The concept of AUTAC originates from studies on selective autophagy triggered by infection, where nitric oxide (NO) and reactive oxygen species (ROS) mediate the degradation of bacterial proteins. Specifically, NO facilitates the conversion of cytoplasmic cyclic guanosine monophosphate (cGMP) to 8-nitro-cGMP, which modifies bacterial surface proteins via S-guanylation, targeting them for autophagic degradation [22,34,49-51]. Takahashi et al. [23] harnessed this pathway to develop the first and second generations of AUTACs, substituting cysteine with a pyrazole ring in the degradation tag. Building on this framework, we developed a second-generation AUTAC to selectively degrade Mcl1. Our findings confirmed the autophagy-dependent mechanism of Mcl1 degradation by AUTAC, validated pharmacologically using early and late autophagy inhibitors (3-MA and CQ, respectively) and genetically via ATG5 knockdown. AUTAC effectively reduced the viability of multiple myeloma and NSCLC cells while sparing cardiac cells—a crucial advantage, as prior Mcl1 inhibitors failed in clinical trials due to cardiac toxicity [33].

AUTAC alone induced autophagic flux in a time-dependent manner, consistent with the effect of 8-nitro-cGMP [22]. We further exploited the cytoprotective autophagy induced by CFZ, repurposing it as a degradation mechanism for Mcl1. The combination of CFZ and AUTAC markedly reduced Mcl1 levels in both wild-type and proteasome inhibitor-resistant multiple myeloma and NSCLC cells, accompanied by a robust upregulation of autophagic flux. Importantly, NRF1 and functional autophagy were essential for Mcl1 degradation, as shown through genetic inhibition approaches. These mechanistic insights translated into significant reductions in cellular viability and increased apoptosis, highlighting the ability of AUTAC to sensitize resistant cells to CFZ.

The interplay between autophagy and PI resistance is well-established [18-20,40], and we confirmed that autophagy inhibition using CQ or BAF augmented CFZ-induced cytotoxicity. However, the lack of selective autophagy inhibitors and the adverse effects of existing agents, such as CQ and HCQ, limit their clinical utility [52-55]. This study introduces a novel strategy of harnessing PIs' cytoprotective autophagy, rather than inhibiting it, by targeting resistance-associated proteins like Mcl1 for autophagic degradation.

Further research is necessary to explore the *in vivo* potential of AUTACs, particularly in preclinical and clinical settings, to fully realize their therapeutic promise. Our findings underscore the feasibility of transforming cytoprotective autophagy into a cell death mechanism, offering a targeted approach to overcoming PI resistance and expanding therapeutic strategies in cancer.

MATERIALS AND METHODS

Cell Culture. MM.1S (CRL-2974; ATCC), RPMI-8226 (CCL-155; ATCC), AMO-1, AMO-1 resistant/ AMO-1^R (both sensitive and resistant cell lines were obtained from Dr. Bianchi Lab, Division of Hematology, Brigham and Women's Hospital, Harvard Medical School), NCI-H1975 [56], NCI-H1975 resistant/ NCI-$H1975^R$ (NCI-H1975 were continuously exposed to increasing concentrations of bortezomib (up to 10 nM) over a period of 10 weeks, with surviving cells maintained in 10 nM), U266B1 resistant/ $U266B1^R$ [57], U266B1 (TIB-196; ATCC), U266B1 $ATG5^{KD}$ [58] and their derivatives were grown in Roswell Park Memorial Institute Medium (RPMI) (Gibco), while AC16 cells (CRL-3568; ATCC) were grown in Dulbecco's Modified Eagle Medium (DMEM; Gibco). Both media were supplemented with 10% fetal bovine serum (FBS; Atlanta Biologicals), 1X penicillin-streptomycin (Pen/Strep; Invitrogen) and 5 µg/ml Plasmocin Prophylactic (PP; InvivoGen). All cell lines were grown at 37°C in a humidified incubator with 5% CO2.

Western blotting. Cells were plated and treated in six-well plates, then collected at the indicated time points and washed once with ice-cold PBS. Cells lysed using RIPA Buffer (20 mM Tris-HCl pH 7.4, 1% sodium deoxycholate, 1% Triton X-100, 0.1% SDS, 150 mM NaCl, and 1 mM EDTA) containing protease and phosphatase Inhibitor cocktail (Cat No: PI78447; Thermo Fisher Scientific), then incubated on ice for 15 min, and centrifuged at 14,000 rpm for 10 min at 4°C. Protein concentrations were measured by the bicinchoninic acid (BCA) assay. Western blot samples were prepared with 4X Laemmli protein sample buffer (Cat No:1610747; Bio-Rad) with the addition of 2-mercaptoethanol on the day of lysis, followed by boiling for 7 min. 10-15 µg of protein was used for SDS-PAGE, gels were transferred onto Immobilon FL PVDF membranes (Cat No: IPVH00010; Millipore Sigma). Membranes were blocked with 5% blotting grade blocker (Cat No: 1706404; BIO-RAD) in TBST for 1-2 h.

Blots were incubated with the indicated primary antibodies overnight, then washed with TBST and incubated with secondary antibodies for 1 h at room temperature. The antibodies used were LC3B (Cat No:2775S; Cell Signaling) at 1:1,000, NRF1 (Cat No:8052S; Cell Signaling) at 1:1,000, cleaved caspase-3 (Cat No:9661L; Cell Signaling) at 1:500, ATG5 (Cat No: 12994S; Cell Signaling) at 1:1000, SQSTM1/p62 (Cat No:5114S; Cell Signaling) at 1:1000, Mcl1 (Cat No: 5453S; Cell Signaling) at 1:500, Bcl2 (Cat No: 3498S; Cell Signaling) at 1:1,000, Bclxl (Cat No: 2764 S; Cell Signaling) at 1:1,000, and GAPDH (Cat No: 5174S; Cell Signaling) at 1:10,000. Goat anti-Rabbit Igg HRP conjugate antibody (Cat No:1706515; BIO-RAD) at 1:10,000 dilutions. Blots then washed with TBST, then incubated with clarity western ECL substrate (Cat No: 1705060; BIO-RAD) for 5 minutes. Imaging of the blots was done by the LiCOR Odyssey Fc Imaging System. Quantification of Western blots was done by Image J software.

Cell viability. The CellTiter-Glo assay was utilized as the screening protocol for drugs action. Cells were plated in 96 well plate at a density of 2500-6000 cells per well and then were treated with the indicated conditions. The CellTiter-Glo assay (G7570; Promega) was performed according to standard protocol and luminescence was quantified using a POLARStar Optima cell microplate reader. The figures were generated using GraphPad Prism software.

Clonogenic assay. Cells plated in 6 well-plates at density of 2500-3000 cells per well, then allowed to adhere overnight. Cells treated with AUTAC 5 µM and/or CFZ (2.5-10 nM) for 72h,

then drug removed, and cells replenished with fresh media every 3 days for total of 9 days. Plates were fixed with methanol, stained with crystal violet, and manually counted. The figures were generated using GraphPad Prism software.

Lysotracker imaging. Cells were plated in 6 well plates and starved (treated with FBS depleted media) or treated with CFZ 10nM for 24h. Cells stained with DAPI (Cat No: PI62249; ThermoFisher) and Lysotracker (Cat No: L7528; ThermoFisher) stains according to the manufacture protocol. Fluorescence images of cells were taken using a brightfield inverted microscope (20X objective, Q-Color3™ Olympus Camera; Olympus, Tokyo, Japan). The merged images and quantification were generated using Image J software. The figures were generated using GraphPad Prism software.

U266B1 NRF1^{KO} cells. Edit-R human NRF1 all-in-one lentivirus sgRNA (Catalog#: SGSH12178-249373759) and Edit-R all-in-one lentiviral sgRNA hEF1a-EGFP non-targeting control (Catalog#: GSGC12062) were purchased from Horizon. For generating lentiviral supernatant, HEX 293 LXT cells were grown to 80% confluency in a 10 cm dish and transfected with lipofectamine (L3000015, ThermoFisher Scientific) with 8 µg lentivirus construct, 6 µg psPAX2 (packaging plasmid, 12260, Addgene), 4 µg pmD2.G (envelope plasmid, 12259, Addgene). Cells were incubated in OptiMEM (31985070, Thermo Fisher Scientific) transfection reagent overnight at 37 °C. The OptiMEM was replaced with fresh 5 mL 5% FBS full media, and cells were incubated at 10% CO_2. 48 hours post-transfection, the supernatant containing virus was harvested and immediately filtered to remove cell debris. U266B1 cells were transduced with lentiviral supernatant supplemented with fresh growth media and 8 µg/mL polybrene. Successfully transduced cells were then selected by fluorescence-activated cell sorting (FACS). To confirm NRF1 knockout in U266B1 cells, WB was performed. U266B1 and U266B1 NRF1^{KO} cells were treated with 10 nM CFZ for 6 hours.

Immunofluorescence. For immunofluorescence (IF), U266B1 WT cells were treated with 5 µM AUTAC for either 24 or 48 hours, or with 10 nM CFZ, 5 µM AUTAC, or a combination of AUTAC and CFZ for 16 hours. The treated cells were seeded onto 12-mm-diameter glass coverslips placed in 12-well culture dishes pre-coated with 0.01% poly-L-lysine (Sigma-Aldrich, P4832) for 1 hour. Cells were washed with PBS before fixation in 4% paraformaldehyde for 30 minutes at room temperature (RT). Following fixation, cells were rinsed with PBS and blocked for 1 hour in a blocking buffer containing 5% BSA and 0.1% Triton X-100 in PBS. The cells were then incubated overnight at 4°C with the designated primary antibodies including LAMP1 (Cat. No. 15665S, Cell Signaling Technology), LC3B (Cat. No. 83506S, Cell Signaling Technology), and Mcl1 (Cat. No. 94296S, Cell Signaling Technology). After three washes with PBS, the cells were incubated with the corresponding secondary antibodies (Alexa Fluor 488 anti-mouse; Lot: 160324, Jackson ImmunoResearch, Alexa Fluor 555 goat anti-mouse IgG; Lot: WA316324, Invitrogen, and Alexa Fluor 594 goat anti-rabbit IgG; Lot: 1608397, Life Technologies). The secondary antibodies were diluted in antibody solution (5% BSA and 0.1% Triton X-100 in PBS) and incubated for 2 hours at room temperature (RT). Nuclear staining was performed by incubating the cells with 4’,6-diamidino-2-phenylindole (DAPI; Lot: WE3286201, Thermo Scientific) for 3 minutes at RT in the dark. Cells were washed three times with PBS, mounted onto glass slides using a mounting medium (Vectashield), and imaged using a Zeiss Laser Scanning Microsope (LSM) 700 fitted with a 63x oil-immersion lens. Images were analyzed, processed and quantified using ImageJ software. The figures were generated using GraphPad Prism software.

Statistical analysis. Unless otherwise indicated, all quantitative data is shown as mean ± SEM from at least three independent experiments, all of which were conducted in triplicates or 6 replicates (cell viability assays). GraphPad Prism 10 software was used for statistical analysis. All data was analyzed using two-way ANOVA, with Tukey or Sidak post hoc.

ACKNOWLEDGEMENTS

This work was supported by a NIH/NIGMS grant R01GM132396 (S.K.R). We thank Gugan Thuduppathy for helpful discussions. Services in support of the research project were generated by the VCU Massey Comprehensive Cancer Center Microscopy Shared Resource, supported, in part, with funding from NIH-NCI Cancer Center Support Grant P30 CA016059.

REFERENCES

1 Moreau, P. *et al.* Proteasome inhibitors in multiple myeloma: 10 years later. *Blood* **120**, 947-959, doi:10.1182/blood-2012-04-403733 (2012).

2 Lee, H. J., Badillo, M., Romaguera, J. & Wang, M. A phase II study of carfilzomib in the treatment of relapsed/refractory mantle cell lymphoma. *British journal of haematology* **184**, 460-462, doi:10.1111/bjh.15107 (2019).

3 Patiño-Escobar, B., Talbot, A. & Wiita, A. P. Overcoming proteasome inhibitor resistance in the immunotherapy era. *Trends in pharmacological sciences* **44**, 507-518, doi:10.1016/j.tips.2023.05.006 (2023).

4 Ito, S. Proteasome Inhibitors for the Treatment of Multiple Myeloma. *Cancers* **12**, doi:10.3390/cancers12020265 (2020).

5 Gu, J. J. *et al.* The novel proteasome inhibitor carfilzomib induces cell cycle arrest, apoptosis and potentiates the anti-tumour activity of chemotherapy in rituximab-resistant lymphoma. *British journal of haematology* **162**, 657-669, doi:10.1111/bjh.12452 (2013).

6 Weyburne, E. S. *et al.* Inhibition of the Proteasome β2 Site Sensitizes Triple-Negative Breast Cancer Cells to β5 Inhibitors and Suppresses Nrf1 Activation. *Cell chemical biology* **24**, 218-230, doi:10.1016/j.chembiol.2016.12.016 (2017).

7 Shah, M. A. *et al.* A multicenter, phase II study of bortezomib (PS-341) in patients with unresectable or metastatic gastric and gastroesophageal junction adenocarcinoma. *Investigational new drugs* **29**, 1475-1481, doi:10.1007/s10637-010-9474-7 (2011).

8 Rosenberg, J. E. *et al.* Phase II study of bortezomib in patients with previously treated advanced urothelial tract transitional cell carcinoma: CALGB 90207. *Annals of oncology : official journal of the European Society for Medical Oncology* **19**, 946-950, doi:10.1093/annonc/mdm600 (2008).

9 Papadopoulos, K. P. *et al.* A phase I/II study of carfilzomib 2-10-min infusion in patients with advanced solid tumors. *Cancer chemotherapy and pharmacology* **72**, 861-868, doi:10.1007/s00280-013-2267-x (2013).

10 Aghajanian, C. *et al.* A phase II evaluation of bortezomib in the treatment of recurrent platinum-sensitive ovarian or primary peritoneal cancer: a Gynecologic Oncology Group study. *Gynecologic oncology* **115**, 215-220, doi:10.1016/j.ygyno.2009.07.023 (2009).

11 Engel, R. H. *et al.* A phase II study of single agent bortezomib in patients with metastatic breast cancer: a single institution experience. *Cancer investigation* **25**, 733-737, doi:10.1080/07357900701506573 (2007).

12 Ge, M. *et al.* Modulating proteasome inhibitor tolerance in multiple myeloma: an alternative strategy to reverse inevitable resistance. *British Journal of Cancer* **124**, 770-776, doi:10.1038/s41416-020-01191-y (2021).

13 Ward, M. A. *et al.* Transcription factor Nrf1 regulates proteotoxic stress-induced autophagy. *The Journal of cell biology* **223**, doi:10.1083/jcb.202306150 (2024).

14 Koizumi, S. *et al.* The aspartyl protease DDI2 activates Nrf1 to compensate for proteasome dysfunction. *eLife* **5**, doi:10.7554/eLife.18357 (2016).

15 Lehrbach, N. J. & Ruvkun, G. Proteasome dysfunction triggers activation of SKN-1A/Nrf1 by the aspartic protease DDI-1. *eLife* **5**, doi:10.7554/eLife.17721 (2016).

16 Wirawan, E., Berghe, T. V., Lippens, S., Agostinis, P. & Vandenabeele, P. Autophagy: for better or for worse. *Cell Research* **22**, 43-61, doi:10.1038/cr.2011.152 (2012).

17 Elshazly, A. M., Wright, P. A., Xu, J. & Gewirtz, D. A. Topoisomerase I poisons-induced autophagy: Cytoprotective, Cytotoxic or Non-protective. *Autophagy reports* **2**, 1-16, doi:10.1080/27694127.2022.2155904 (2023).

18 Jarauta, V. *et al.* Inhibition of autophagy with chloroquine potentiates carfilzomib-induced apoptosis in myeloma cells in vitro and in vivo. *Cancer letters* **382**, 1-10, doi:10.1016/j.canlet.2016.08.019 (2016).
19 Riz, I., Hawley, T. S. & Hawley, R. G. KLF4-SQSTM1/p62-associated prosurvival autophagy contributes to carfilzomib resistance in multiple myeloma models. *Oncotarget* **6**, 14814-14831, doi:10.18632/oncotarget.4530 (2015).
20 Chavda, S. J. *et al.* Autophagy Blockade Disrupts Myeloma Cell Recovery from Proteasome Inhibition and Enhances Apoptosis. *Blood* **138**, 1567, doi:https://doi.org/10.1182/blood-2021-146400 (2021).
21 Salimi, A. *et al.* Targeting autophagy increases the efficacy of proteasome inhibitor treatment in multiple myeloma by induction of apoptosis and activation of JNK. *BMC Cancer* **22**, 735, doi:10.1186/s12885-022-09775-y (2022).
22 Ito, C. *et al.* Endogenous nitrated nucleotide is a key mediator of autophagy and innate defense against bacteria. *Molecular cell* **52**, 794-804, doi:10.1016/j.molcel.2013.10.024 (2013).
23 Takahashi, D. *et al.* AUTACs: Cargo-Specific Degraders Using Selective Autophagy. *Molecular cell* **76**, 797-810.e710, doi:10.1016/j.molcel.2019.09.009 (2019).
24 Wang, H., Guo, M., Wei, H. & Chen, Y. Targeting MCL-1 in cancer: current status and perspectives. *Journal of Hematology & Oncology* **14**, 67, doi:10.1186/s13045-021-01079-1 (2021).
25 Lucendo, E. *et al.* Mcl-1 and Bok transmembrane domains: Unexpected players in the modulation of apoptosis. *Proceedings of the National Academy of Sciences* **117**, 27980-27988, doi:doi:10.1073/pnas.2008885117 (2020).
26 Al-Odat, O. *et al.* Mcl-1 Inhibition: Managing Malignancy in Multiple Myeloma. *Frontiers in pharmacology* **12**, 699629, doi:10.3389/fphar.2021.699629 (2021).
27 Tron, A. E. *et al.* Discovery of Mcl-1-specific inhibitor AZD5991 and preclinical activity in multiple myeloma and acute myeloid leukemia. *Nature Communications* **9**, 5341, doi:10.1038/s41467-018-07551-w (2018).
28 Zhou, W. *et al.* Small interfering RNA targeting mcl-1 enhances proteasome inhibitor-induced apoptosis in various solid malignant tumors. *BMC Cancer* **11**, 485, doi:10.1186/1471-2407-11-485 (2011).
29 Nencioni, A. *et al.* Evidence for a protective role of Mcl-1 in proteasome inhibitor-induced apoptosis. *Blood* **105**, 3255-3262, doi:https://doi.org/10.1182/blood-2004-10-3984 (2005).
30 Al-Odat, O. S. *et al.* KS18, a Mcl-1 inhibitor, improves the effectiveness of bortezomib and overcomes resistance in refractory multiple myeloma by triggering intrinsic apoptosis. *Frontiers in pharmacology* **15**, 1436786, doi:10.3389/fphar.2024.1436786 (2024).
31 Ponder, K. G. *et al.* Dual inhibition of Mcl-1 by the combination of carfilzomib and TG02 in multiple myeloma. *Cancer biology & therapy* **17**, 769-777, doi:10.1080/15384047.2016.1192086 (2016).
32 Bolomsky, A. *et al.* Heterogeneous modulation of Bcl-2 family members and drug efflux mediate MCL-1 inhibitor resistance in multiple myeloma. *Blood advances* **5**, 4125-4139, doi:10.1182/bloodadvances.2020003826 (2021).
33 Bolomsky, A. *et al.* MCL-1 inhibitors, fast-lane development of a new class of anti-cancer agents. *Journal of Hematology & Oncology* **13**, 173, doi:10.1186/s13045-020-01007-9 (2020).
34 Takahashi, D. *et al.* Second-Generation AUTACs for Targeted Autophagic Degradation. *Journal of medicinal chemistry* **66**, 12342-12372, doi:10.1021/acs.jmedchem.3c00861 (2023).
35 Wang, Z. *et al.* Proteolysis Targeting Chimeras for the Selective Degradation of Mcl-1/Bcl-2 Derived from Nonselective Target Binding Ligands. *Journal of medicinal chemistry* **62**, 8152-8163, doi:10.1021/acs.jmedchem.9b00919 (2019).

36 Mauthe, M. *et al.* Chloroquine inhibits autophagic flux by decreasing autophagosome-lysosome fusion. *Autophagy* **14**, 1435-1455, doi:10.1080/15548627.2018.1474314 (2018).
37 Seglen, P. O. & Gordon, P. B. 3-Methyladenine: specific inhibitor of autophagic/lysosomal protein degradation in isolated rat hepatocytes. *Proceedings of the National Academy of Sciences* **79**, 1889-1892 (1982).
38 Shang, L. *et al.* Nutrient starvation elicits an acute autophagic response mediated by Ulk1 dephosphorylation and its subsequent dissociation from AMPK. *Proceedings of the National Academy of Sciences of the United States of America* **108**, 4788-4793, doi:10.1073/pnas.1100844108 (2011).
39 Fostier, K., De Becker, A. & Schots, R. Carfilzomib: a novel treatment in relapsed and refractory multiple myeloma. *OncoTargets and therapy* **5**, 237-244, doi:10.2147/ott.S28911 (2012).
40 Zang, Y. *et al.* The next generation proteasome inhibitors carfilzomib and oprozomib activate prosurvival autophagy via induction of the unfolded protein response and ATF4. *Autophagy* **8**, 1873-1874, doi:10.4161/auto.22185 (2012).
41 Radhakrishnan, S. K. *et al.* Transcription factor Nrf1 mediates the proteasome recovery pathway after proteasome inhibition in mammalian cells. *Molecular cell* **38**, 17-28, doi:10.1016/j.molcel.2010.02.029 (2010).
42 Radhakrishnan, S. K., den Besten, W. & Deshaies, R. J. p97-dependent retrotranslocation and proteolytic processing govern formation of active Nrf1 upon proteasome inhibition. *eLife* **3**, e01856 (2014).
43 Vangala, J. R. & Radhakrishnan, S. K. Nrf1-mediated transcriptional regulation of the proteasome requires a functional TIP60 complex. *The Journal of biological chemistry* **294**, 2036-2045, doi:10.1074/jbc.RA118.006290 (2019).
44 Vangala, J. R., Sotzny, F., Krüger, E., Deshaies, R. J. & Radhakrishnan, S. K. Nrf1 can be processed and activated in a proteasome-independent manner. *Current biology : CB* **26**, R834-r835, doi:10.1016/j.cub.2016.08.008 (2016).
45 Bai, Z. *et al.* Autophagy and cancer treatment: four functional forms of autophagy and their therapeutic applications. *J Zhejiang Univ Sci B* **23**, 89-101, doi:10.1631/jzus.B2100804 (2022).
46 Gewirtz, D. A. The four faces of autophagy: implications for cancer therapy. *Cancer Res* **74**, 647-651, doi:10.1158/0008-5472.Can-13-2966 (2014).
47 Elshazly, A. M. *et al.* Is Autophagy Targeting a Valid Adjuvant Strategy in Conjunction with Tyrosine Kinase Inhibitors? *Cancers* **16**, 2989 (2024).
48 Manasanch, E. E. & Orlowski, R. Z. Proteasome inhibitors in cancer therapy. *Nature reviews. Clinical oncology* **14**, 417-433, doi:10.1038/nrclinonc.2016.206 (2017).
49 Nakagawa, I. *et al.* Autophagy defends cells against invading group A Streptococcus. *Science* **306**, 1037-1040 (2004).
50 Sawa, T. *et al.* Protein S-guanylation by the biological signal 8-nitroguanosine 3′, 5′-cyclic monophosphate. *Nature chemical biology* **3**, 727-735 (2007).
51 Lu, S.-L. *et al.* Endothelial cells are intrinsically defective in xenophagy of Streptococcus pyogenes. *PLoS pathogens* **13**, e1006444 (2017).
52 Elshazly, A. M. & Gewirtz, D. A. Is Autophagy Inhibition in Combination with Temozolomide a Therapeutically Viable Strategy? *Cells* **12**, doi:10.3390/cells12040535 (2023).
53 Manzo, C., Gareri, P. & Castagna, A. Psychomotor Agitation Following Treatment with Hydroxychloroquine. *Drug safety - case reports* **4**, 6, doi:10.1007/s40800-017-0048-x (2017).
54 Xu, H., Zhang, X. Y., Wang, W. W. & Wang, J. Hydroxychloroquine Increased Anxiety-Like Behaviors and Disrupted the Expression of Some Related Genes in the Mouse Brain. *Frontiers in pharmacology* **12**, 633112, doi:10.3389/fphar.2021.633112 (2021).

55 Naddaf, E., Paul, P. & AbouEzzeddine, O. F. Chloroquine and Hydroxychloroquine Myopathy: Clinical Spectrum and Treatment Outcomes. *Frontiers in neurology* **11**, 616075, doi:10.3389/fneur.2020.616075 (2020).

56 Chougoni, K. K. *et al.* Oncogenic Mutant p53 Sensitizes Non–Small Cell Lung Cancer Cells to Proteasome Inhibition via Oxidative Stress–Dependent Induction of Mitochondrial Apoptosis. *Cancer Research Communications* **4**, 2685-2698, doi:10.1158/2767-9764.Crc-23-0637 (2024).

57 Li, L. *et al.* Non-canonical role for the ataxia-telangiectasia-Rad3 pathway in STAT3 activation in human multiple myeloma cells. *Cellular oncology (Dordrecht, Netherlands)* **46**, 1369-1380, doi:10.1007/s13402-023-00817-6 (2023).

58 Chen, S. *et al.* Targeting SQSTM1/p62 induces cargo loading failure and converts autophagy to apoptosis via NBK/Bik. *Molecular and cellular biology* **34**, 3435-3449, doi:10.1128/mcb.01383-13 (2014).

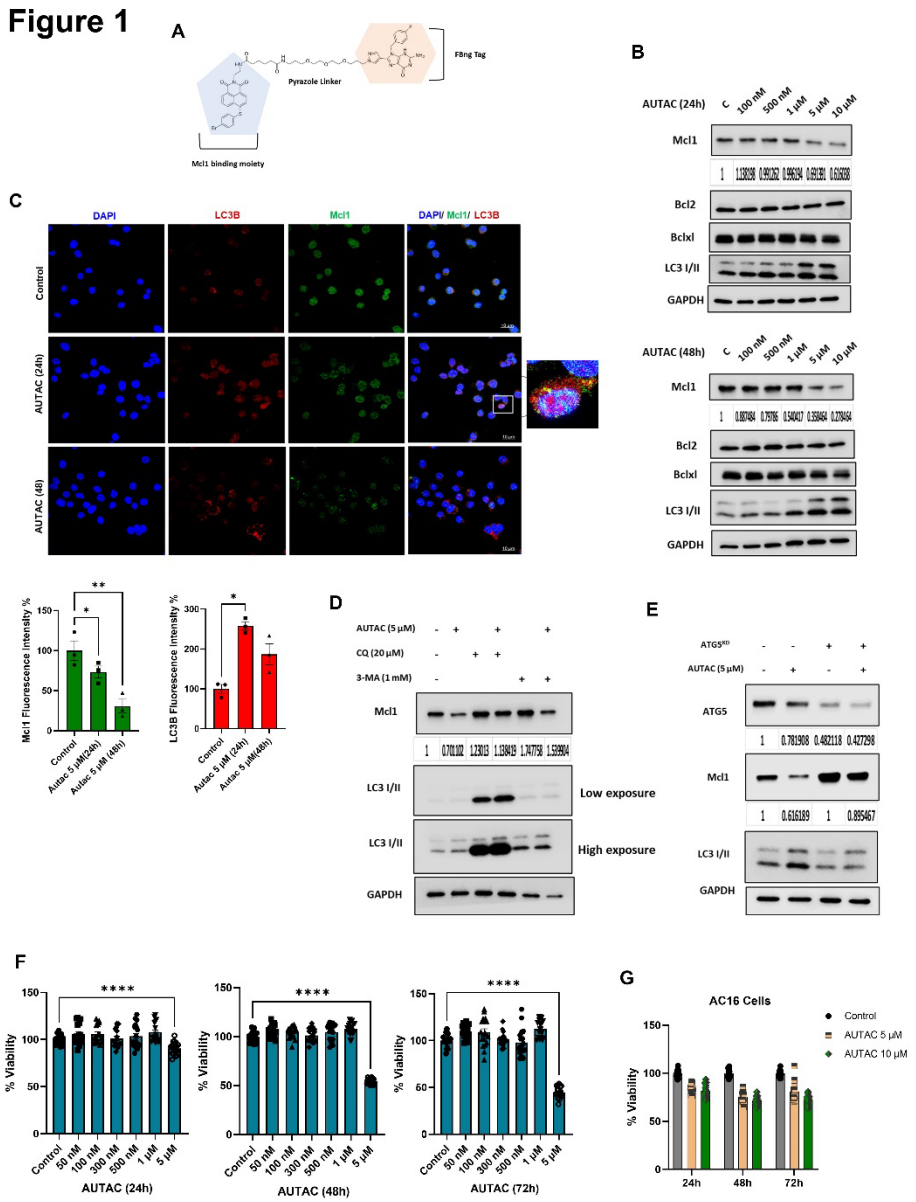

Figure 1. AUTAC degrades Mcl1 through autophagy. (A) The chemical structure of Mcl1-specific AUTAC consists of a MCL1 binding moiety connected to a FBnG-tag via a pyrazole linker. **(B)** Western blot analysis for Mcl1, Bcl2, Bclxl, and LC3I/II proteins in U266B1 cells treated with the indicated concentrations of AUTAC for 24h and 48h. GAPDH was used as the loading control. **(C)** Confocal images with their quantification for Mcl1 and LC3B proteins in U266B1 cells treated with AUTAC (5 µM) for 24 and 48h (scale 10 µM). **(D)** Western blot analysis for Mcl1, and LC3I/II proteins in U266B1 cells treated with different combinations of AUTAC (5 µM), CQ (20 µM) or 3-MA (1 mM) for 24h. GAPDH was used as the loading control. **(E)** Western blot analysis for ATG5, Mcl1, and LC3I/II proteins in U266B1 wild-type and U266B1 $ATG5^{KD}$ cells treated with AUTAC (5 µM) for 24h. GAPDH was used as the loading control. **(F)** The percentage of cellular viability for U266B1 cells treated with the indicated concentrations AUTAC for 24, 48 and 72h. **(G)** Viability of AC16 cardiomyocytes treated with the indicated concentrations of AUTAC for 24, 48 and 72h.

Three biological replicates for each cell line were used to perform cell viability assay and Western blotting. * $p < 0.05$, ** $p < 0.01$, and **** $p < 0.0001$ indicates statistical significance of each condition compared to the indicated control as determined using two-way ANOVA with Sidak's post hoc test.

Figure 2

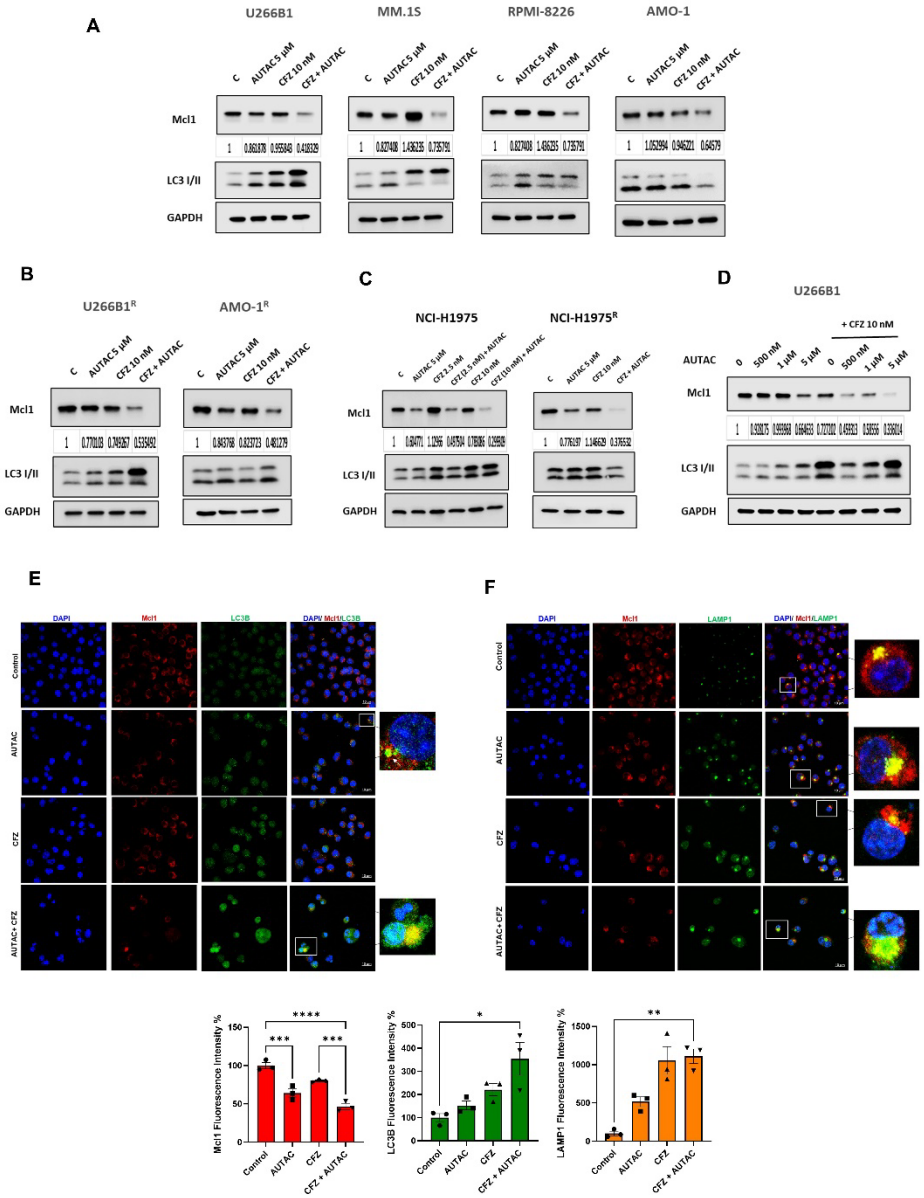

Figure 2. Carfilzomib enhances AUTAC-mediated MCL1 degradation in multiple myeloma and non-small cell lung cancer cells. (A) Western blot analysis for Mcl1, and LC3I/II proteins in U266B1, MM.1S, RPMI-8226 and AMO-1 cells treated with AUTAC (5 μM) and/or CFZ (10 nM) for 16h, except for AMO-1 cells treated for 24h. GAPDH was used as the loading control. **(B)** Western blot analysis for Mcl1, and LC3I/II proteins in U266B1^{R} and AMO-1^{R} cells treated with AUTAC (5 μM) for 48h, then CFZ (10 nM) was added for the last 24h. GAPDH was used as the loading control. **(C)** Western blot analysis for Mcl1, and LC3I/II proteins in NCI-H1975 and NCI-H1975^{R} cells treated with AUTAC (5 μM) and/or CFZ (2.5 nM, and 10 nM) for 72h. GAPDH was used as the loading control. **(D)** Western blot analysis for Mcl1, and LC3I/II proteins in U266B1 cells treated with the indicated concentrations of AUTAC and/or CFZ (10 nM) for 16h. GAPDH was used as the loading control. **(E and F)** Confocal images and their quantification for Mcl1, LC3B (E) and LAMP1 (F) proteins in U266B1 treated with AUTAC (5 μM) and/or CFZ (10 nM) for 16h (scale 10 μM).

Three biological replicates for each cell line were used to perform Western blotting. * $p < 0.05$, ** $p < 0.01$, *** $p < 0.001$ and **** $p < 0.0001$ indicates statistical significance of each condition compared to the indicated control/treatment as determined using two-way ANOVA with Sidak's post hoc test.

Figure 3

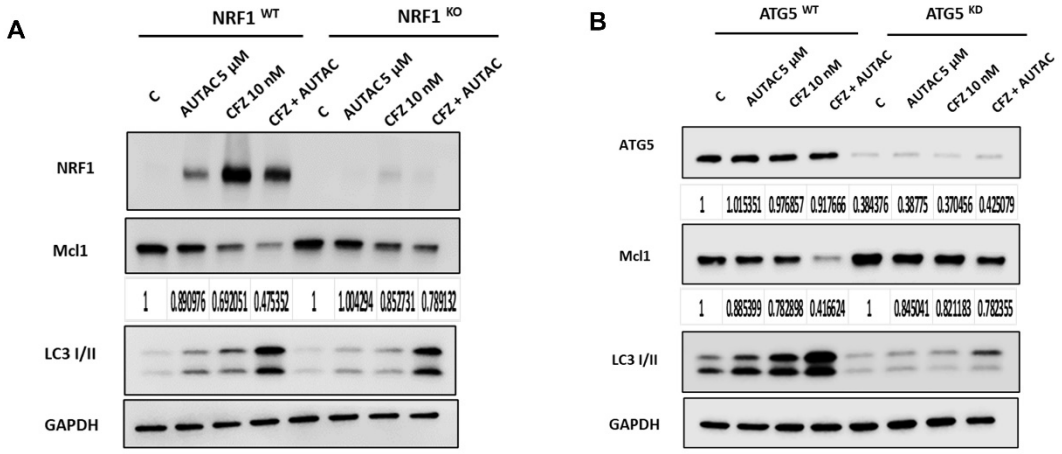

Figure 3. Carfilzomib-mediated potentiation of AUTAC activity is dependent on NRF1 and functional autophagy. (A) Western blot analysis for NRF1, Mcl1, and LC3I/II proteins in U266B1 WT and U266B1 NRF1^{KO} cell lines treated with AUTAC (5 µM) and/or CFZ (10 nM) for 16h. GAPDH was used as the loading control **(B)** Western blot analysis for ATG5, Mcl1, and LC3I/II proteins in U266B1^{WT} and U266B1 ATG5 ^{KD} cell lines treated with AUTAC (5 µM) and/or CFZ (10 nM) for 16h. GAPDH was used as the loading control. Three biological replicates for each cell line were used to perform Western blotting.

Figure 4

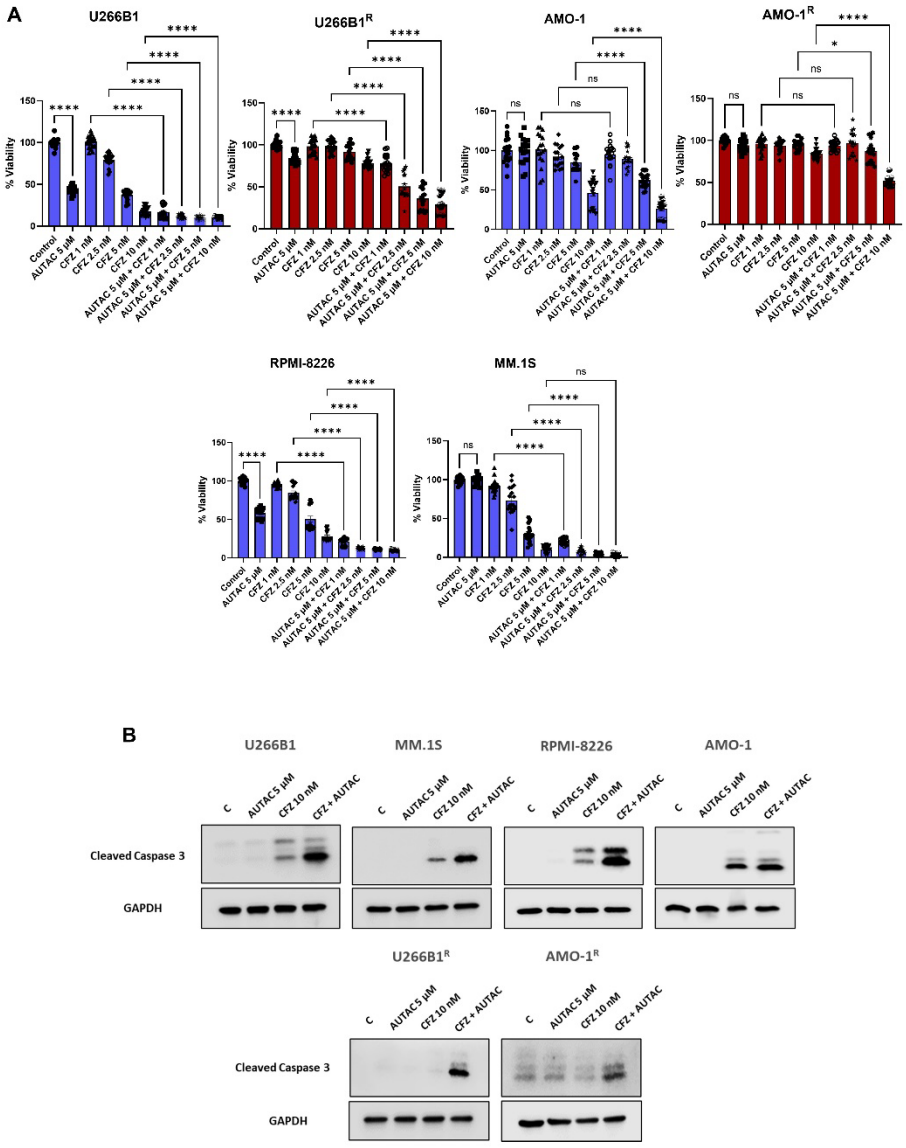

Figure 4. Carfilzomib in combination with AUTAC synergistically induces cell death in wild-type and proteasome inhibitor-resistant multiple myeloma cells. (A) The percentage of cellular viability for U266B1, MM.1S, AMO-1, RPMI-8226, U266B1^R and AMO-1^R cell lines treated with AUTAC (5 µM) for 72h, then the indicated concentrations of CFZ were added for the last 24h. **(B)** Western blot analysis for cleaved caspase 3 protein in multiple myeloma cell lines after 16h (U266B1, MM.1S, RPMI-8226), and 24h (AMO-1) treatment with AUTAC (5 µM) and/or CFZ (10 nM), while U266B1^R and AMO-1^R cells treated for 48h with AUTAC (5 µM), then CFZ (10 nM) was added for the last 24h. GAPDH was used as the loading control.

Three biological replicates for each cell line were used to perform cell viability assay and Western blotting. ns indicates non-statistical significance, while * $p < 0.05$, and **** $p < 0.0001$ indicates statistical significance of each

condition compared to the indicated control/treatment as determined using two-way ANOVA with Sidak's post hoc test.

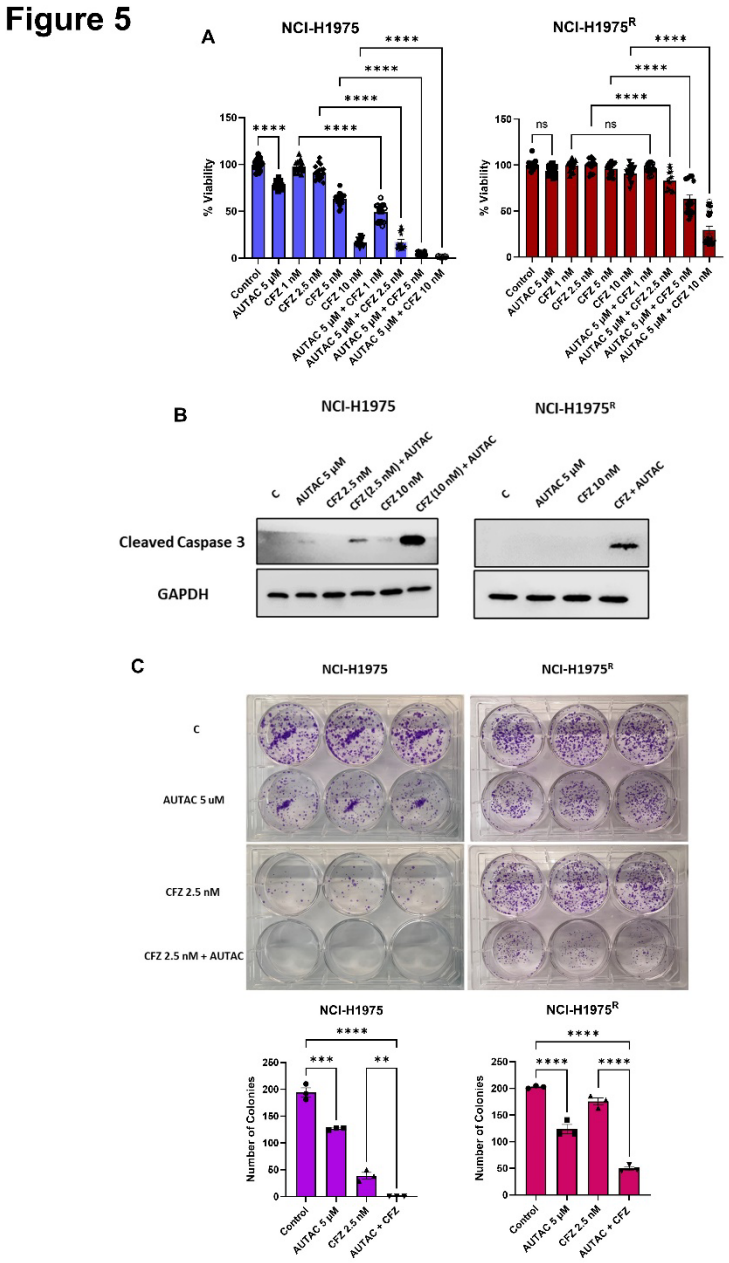

Figure 5. The impact of combining carfilzomib with AUTAC in wild-type and proteasome inhibitor-resistant non-small cell lung cancer cells. (A) The percentage of cellular viability for NCI-H1975 and NCI-H1975^R cells treated with AUTAC (5 μM) and/or the indicated concentrations of CFZ for 72h. **(B)** Western blot analysis for cleaved caspase 3 protein in NCI-H1975 and NCI-H1975^R cells treated with AUTAC (5 μM) and/or CFZ (2.5, and 10 nM) for 72h. GAPDH was used as the loading control **(C)** Colony formation assay and its quantification for NCI-H1975 and NCI-H1975^R cells treated with AUTAC (5 μM) and/or CFZ (2.5, and 10 nM) for 72h, then supplemented with media every three days for total 9 days.

Three biological replicates for each cell line were used to perform cell viability assay, colony formation assay and Western blotting. ns indicates non-statistical significance, while ** $p < 0.01$, *** $p < 0.001$ and **** $p < 0.0001$ indicates statistical significance of each condition compared to the indicated control/treatment as determined using two-way ANOVA with Sidak's post hoc test.

Supplementary Figure 1

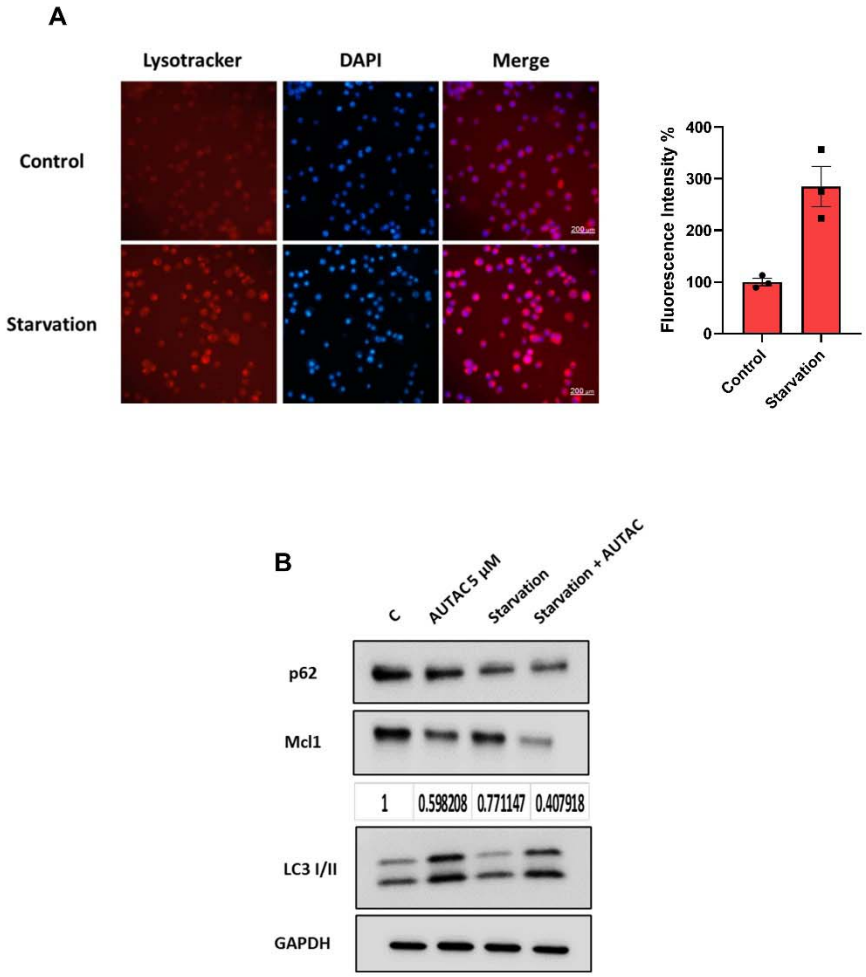

Supplementary Figure 1. Autophagy induction via starvation augments the Mcl1 degradation ability of AUTAC. (A) Representative florescence microscopy images and their quantification for U266B1 cells subjected to starvation for 24h, then the cells stained with DAPI and lysotracker stain. All images were generated under the same magnification (20X). **(B)** Western blot analysis for p62, Mcl1, and LC3I/II proteins in U266B1 starved and treated with AUTAC (5 µM) for 24h. GAPDH was used as the loading control. Three biological replicates for each cell line were used to perform Western blotting.

Supplementary Figure 2

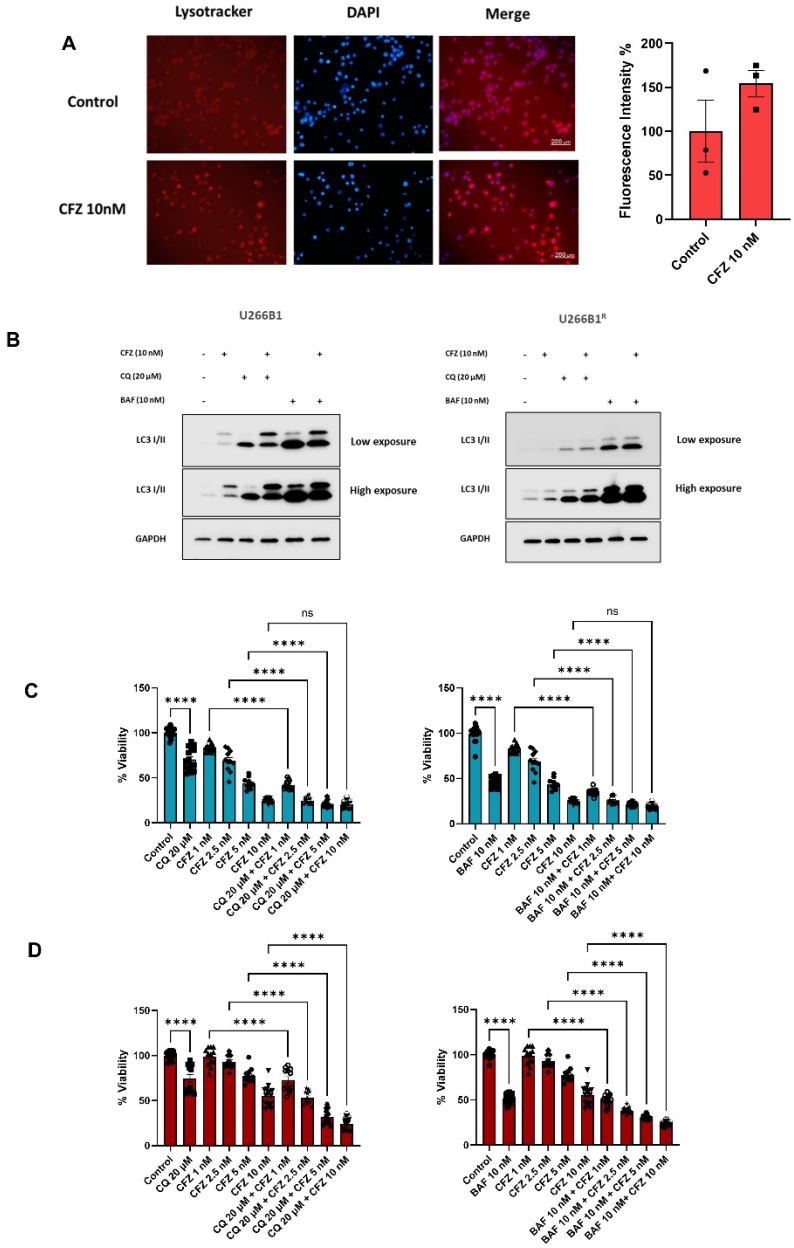

Supplementary Figure 2. Carfilzomib induces a cytoprotective autophagy in multiple myeloma cells. (A) Representative florescence microscopy images with their quantification for U266B1 cells treated with carfilzomib (10 nM) for 24h, then the cells stained with DAPI and lysotracker stain. All images were generated under the same magnification (20X). **(B)** Western blot analysis for LC3I/II protein in U266B1 and U266B1^{R} treated with carfilzomib (10 nM) and/or CQ (20 μM) or bafilomycin (10 nM) for 24h. GAPDH was used as the loading control. **(C and D)** The percentage of cellular viability for U266B1 and U266B1^{R} cells treated with (C) CQ (20 μM) or (D) bafilomycin (10 nM) for 72h, then the indicated concentrations of CFZ were added for the last 24h.

Three biological replicates for each cell line were used to perform cell viability assay, and Western blotting. ns indicates non-statistical significance, while **** $p < 0.0001$ indicates statistical significance of each condition compared to the indicated control/treatment as determined using two-way ANOVA with Sidak's post hoc test.